Convection in the east Pacific intertropical convergence zone

David J. Raymond[1]

Key points:
- The east Pacific ITCZ occurs in a region of strong meridional SST gradient.
- Boundary layer convergence drives a shallow circulation in this region.
- Thermodynamic factors control deep convection there.

The eastern tropical Pacific exhibits a strong, cross-equatorial sea surface temperature (SST) gradient, which drives a southerly flow in the atmospheric boundary layer. Convergence in this flow is generally considered to drive deep convection in the east Pacific intertropical convergence zone (ITCZ). However, results from cloud modeling and recent field programs provide an alternative thermodynamic mechanism for controlling this convection. While shallow convection responds to boundary layer convergence, deep convection appears to be controlled by a combination of convective inhibition, surface moist entropy fluxes, tropospheric relative humidity, and moist convective instability. These factors explain the sharp minimum in infrared brightness temperature near 8° N while boundary layer convergence occurs over a much broader range of latitudes.

1. Introduction

The east Pacific ITCZ was studied extensively in EPIC2001 (East Pacific Investigation of Climate) [*Raymond et al.*, 2004]. These observations allowed us to derive a clear picture of the latitudinal structure and the temporal variation of the Hadley circulation north of the equator and the associated ITCZ. Though the mean latitude of the ITCZ was near 8° N during this period, it varied between 6° N and 12° N [*Raymond et al.*, 2006], with higher latitude excursions being associated with easterly wave passages or developing tropical cyclones [*Petersen et al.*, 2003].

Shallow and deep Hadley cell modes were found in conjunction with the ITCZ [*Zhang et al.*, 2004]. The former exhibited a northerly return flow back across the equator centered near 850 hPa while the latter was characterized by a return flow in the upper troposphere. The elevation of the return flow reflected the depth of the corresponding convection in the ITCZ. At times the actual flow was a mixture of the two modes. The shallow mode was most prominent in convectively suppressed cases whereas the deep mode dominated during the passage of easterly waves or incipient tropical cyclones.

The question remains as to how convection is forced in the ITCZ. A broadly accepted hypothesis is that this forcing results from convergence in the boundary layer flow driven by the SST gradient. This flow is often approximated as the Ekman balance flow resulting from horizontal pressure gradients in the boundary layer, which in turn are related to spatial variations in the SST. Many of these models are enhanced by the incorporation of momentum transfer from above the boundary layer or by other mechanisms [*Riehl et al.*, 1951; *Lindzen and Nigam*, 1987; *Battisti et al.*, 1999; *Tomas et al.*, 1999; *Stevens et al.*, 2002; *Back and Bretherton*, 2009a].

An alternative point of view, based on the ideas of *Emanuel* [1986, 1987], *Neelin et al.* [1987], and *Yano and Emanuel* [1991], is that surface moist entropy fluxes drive convection, with stronger boundary layer winds resulting in stronger fluxes. This is often referred to as the WISHE (Wind-Induced Surface Heat Exchange) hypothesis [*Yano and Emanuel*, 1991]. A refinement of these ideas invoking the balance between surface fluxes and convective downdrafts in the moist entropy budget [*Raymond*, 1995; *Emanuel*, 1995] was employed by *Raymond et al.* [2006] to explain the time variability of convection in the east Pacific ITCZ.

More recent work has shown that two additional factors are related to the mean intensity of convection in this region (as measured by average rainfall rate), the saturation fraction or column relative humidity, defined as the tropospheric precipitable water divided by the saturated precipitable water,

$$S = \int r \, dp \left/ \int r^* \, dp \right. , \qquad (1)$$

and the instability index,

$$I = s^*_{lo} - s^*_{hi}. \qquad (2)$$

The instability index is a measure of moist convective instability, with moist neutral conditions yielding $I = 0$ [*Bretherton et al.*, 2004; *Peters and Neelin*, 2006; *Raymond and Sessions*, 2007; *Gjorgjievska and Raymond*, 2014; *Raymond et al.*, 2014; *Raymond and Flores*, 2016]. The quantity r in the saturation fraction is the water vapor mixing ratio, r^* is the saturated mixing ratio, and p is the pressure. In the instability index, s^* is the saturated moist entropy, the subscript lo indicates a height

[1]Physics Department and Geophysical Research Center, New Mexico Tech, Socorro, New Mexico, USA.

average over $[1, 3]$ km, and the subscript hi indicates an average over $[5, 7]$ km. Rainfall tends to increase with stronger surface moist entropy fluxes and larger saturation fraction. However, *smaller* values of instability index (down to some limit) tend to produce more rainfall, as the above-cited works show. This somewhat counterintuitive result may provide a partial explanation for the latitudinal preference and variability of the east Pacific ITCZ.

The deep convective inhibition (DCIN) was also found by *Raymond et al.* [2003] to be a factor in the control of convection in the east Pacific. This is defined

$$\text{DCIN} = s_t - s_b \qquad (3)$$

where s_b is the moist entropy averaged over the $[900, 1000]$ hPa layer and s_t is the saturated moist entropy in the $[810, 830]$ hPa layer. It comes into play particularly in regions of lower SST.

In strongly convective situations, the saturation fraction and the instability index are not independent [*Gjorgjievska and Raymond*, 2014]. Due to cloud processes described by *Singh and O'Gorman* [2013], an anticorrelation exists between moist instability and tropospheric relative humidity in strong convection. This occurs because ascending cloud parcels must have greater initial buoyancy to maintain positive buoyancy upon mixing with a drier enviroment. *Raymond et al.* [2014] refer to this as the principle of moisture quasi-equilibrium. Thus, in strong convection, the mean precipitation rate appears to be governed by only three factors, the deep convective inhibition, the surface moist entropy flux, and the instability index, the last of which encompasses the effects of saturation fraction as well. In weaker convection, moisture quasi-equilibrium takes too long to establish itself and the saturation fraction retains an independent role [*Raymond*, 2000]. In this case there is an upper bound on the saturation fraction which decreases with
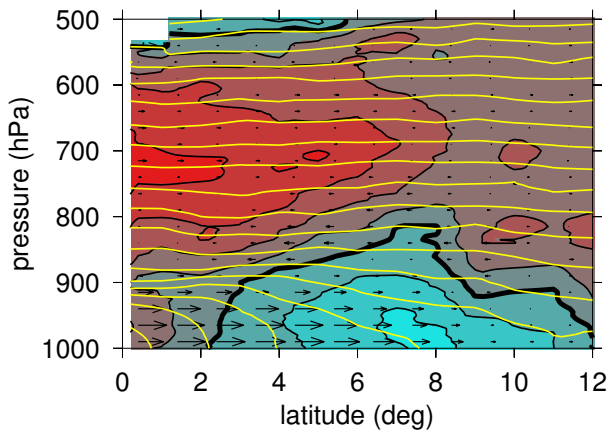
Figure 1. Mean conditions along $95°$ W from EPIC2001 observations. Black contours indicate zonal wind at 2 m s^{-1} intervals with the heavy contour indicating zero wind. Blue and red shades indicate westerlies and easterlies respectively. Arrows indicate the meridional wind with a scale of 10 m s^{-1} deg^{-1}. The yellow contours indicate potential temperature with a 2 K contour interval.

increasing instability index [*Singh and O'Gorman*, 2013; *Raymond and Flores*, 2016].

The variance in the surface entropy flux is associated primarily with boundary layer wind speed variations, whereas according to *Raymond et al.* [2015], the variations in the instability index are a consequence of the balanced thermal response to variations in the vorticity distribution. This comes about as a result of the thermal wind associated with the shear in the tangential wind above and below the vorticity maximum. Persistent large values of DCIN in the east Pacific are generally associated with low SSTs.

The purpose of this paper is to determine whether the above factors can explain the mean latitudinal distribution of deep convection in the tropical east Pacific. Dropsonde observations obtained during EPIC2001 constitute the primary data source for this analysis.

2. Data and methods

In EPIC2001, dropsondes were deployed in repeated traverses between $12°$ N and the equator along $95°$ W using the National Center for Atmospheric Research's C-130 aircraft over a 6-week period in September-October 2001. For 3 of these weeks, the National Oceanic and Atmospheric Administration's ship *R/V Ron Brown* launched radiosondes 6 times per day at ($95°$ W, $10°$ N). It also carried a C-band scanning Doppler radar that was used to characterize the convection.

Raymond et al. [2003] compiled the results of 8 C-130 traversals along $95°$ W including information from the dropsondes as well as SSTs and satellite infrared brightness temperatures along the aircraft trajectory. The C-130 flew the traversals at just above 500 hPa, so sounding results are available from the surface to 500 hPa. Dropsondes were deployed approximately every $1°$ of latitude and the results were interpolated to 5 hPa intervals. For more details, see *Raymond et al.* [2003] and *Raymond et al.* [2006].

The saturation fraction and instability index were computed as a function of latitude for all flights. Due to the flight level of the aircraft, the value of s_{hi}^* was taken as the value of the saturated moist entropy at 500 hPa in the computation of instability index. The value of s_{lo}^* was taken as the average value of the saturated entropy in the pressure range $[700, 900]$ hPa.

The surface moist entropy flux E was calculated using a simple bulk formula with a constant transfer coefficient $C_D = 0.0012$,

$$E = \rho_b C_D (s_{ss}^* - s_b)(U_b^2 + W^2)^{1/2}, \qquad (4)$$

where ρ_b is the air density in the boundary layer ($[970, 1020]$ hPa), s_b and U_b are the boundary layer moist entropy and wind speed, s_{ss}^* is the saturated sea surface moist entropy, and $W = 3$ m s^{-1} is a gustiness correction [*Miller et al.*, 1992].

Raymond and Flores [2016] explored the thermodynamic control of rainfall in a large set of weak temperature gradient cloud resolving model runs [*Raymond and Zeng*, 2005; *Herman and Raymond*, 2014; *Daleu et al.*, 2015] and derived an empirical equation for rainfall rate as a function of three parameters: surface moist entropy flux (E), instability index (I) and saturation fraction (S):

$$R_3 = -28 + 36.4E - 2.67I + 83.3S \quad \text{mm d}^{-1}. \quad (5)$$

Raymond and Flores [2016] found that moisture quasi-equilibrium allowed the saturation fraction to be omitted from the regression leading to this equation. However, the saturation fraction is retained in this work as convection south of the ITCZ may not be strong enough to enforce moisture quasi-equilibrium.

Comparison with observations suggest that this equation overestimates the rainfall by a factor of ≈ 2-3, an error possibly attributable to the use of two-dimensional calculations with a crude cloud physics scheme employed in the derivation of this relationship. In spite of this, the model results show significant skill in predicting averaged rainfall rates when the above correction factor is taken into account [*Raymond and Flores*, 2016].

Two circumstances are not accounted for by the analysis of *Raymond and Flores* [2016]. First, though smaller values of instability index tend to yield larger rainfall rates, there is a lower limit to this dependence, since negative values of instability index represent a convectively stable environment. This limit needs further observational and theoretical investigation, but for the present work, the rainfall is set to zero if $I < 0$. Second, strongly positive values of DCIN are also likely to suppress deep convection, as it becomes difficult to lift parcels out of the planetary boundary layer in this case. Rainfall is suppressed when DCIN > 20 J K^{-1} kg^{-1}. Results do not vary qualitatively for cutoff values in the range $-5 < I < 5$ J K^{-1} kg^{-1} and $10 <$ DCIN < 30 J K^{-1} kg^{-1}. After deriving the rainfall pattern for each traverse, the average values of all quantities from the 8 C-130 traverses are computed.

3. Results

Figure 1 shows the average wind and potential temperature structure along $95°$ W. Strong meridional potential temperature gradients exist below 800 hPa due to the SST gradient, with weak potential temperature gradients above. Strong southerly winds below 900 hPa terminate near $8°$ N, which is also the point of maximum westerlies in the zonal flow. A weak northerly return flow exists between 800 hPa and 900 hPa and an easterly jet exists over the equator with a maximum at 700 hPa.

Figure 2 shows various time-averaged quantities plotted as a function of latitude. The SST, shown in the upper left panel, has its strongest latitudinal gradients south of $3°$ N, with water $27°$ C or greater north of this point. However, as the plot of deep convective inhibition (upper right) shows, DCIN values remain prohibitively large for deep convection to occur until $4°$-$6°$ N. The boundary layer meridional wind ([970, 1020] hPa; lower left) exhibits approximately uniform convergence with latitude over the range [4, 10] N, with minor fluctuations. In spite of this, the infrared brightness temperature (lower right) exhibits a sharp minimum near $8°$ N, indicating a strong preference for convection at this latitude. If convection were forced solely by boundary layer convergence, one would expect a much broader distribution of low infrared brightness temperature with latitude.

Figure 3 shows plots of parameters pertinent to the thermodynamic forcing hypothesis for deep convection. The upper left plot shows the saturation fraction as a function of latitude, averaged over the 8 cases. This quantity peaks near $8°$ N, which coincides with the minimum in infrared brightness temperature. The instability index (upper right) exhibits a low value of about 5 J K^{-1} kg^{-1}

over the range $[2°, 8°]$ N and then increases dramatically with increasing latitude. The surface moist entropy flux (lower left) is large south of $6°$ N and then decreases dramatically north of this point. The rainfall R_3 is plotted in the lower right panel of figure 3. Note that it is similar in form to the infrared brightness temperature plot in figure 2, peaking sharply near $7°$ N, which is only $1°$ south of the minimum in the brightness temperature. This similarity strongly suggests that the computed rainfall R_3 is
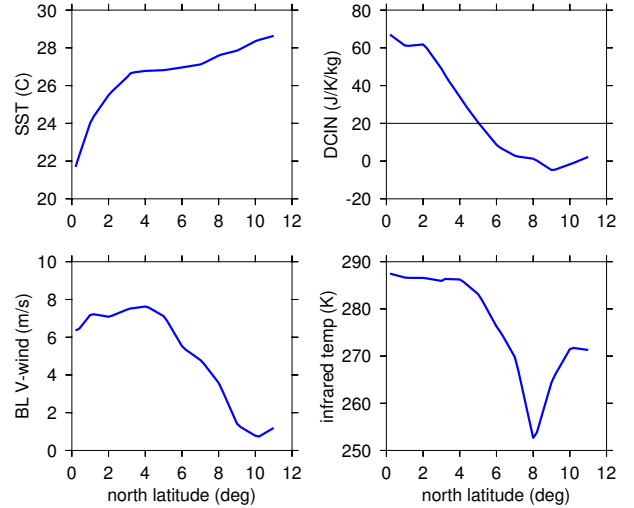
Figure 2. Time-averaged values of SST (upper left), DCIN (upper right), boundary layer meridional wind (lower left), and infrared brightness temperature (lower right) as a function of latitude. The black horizontal line in the DCIN plot shows the assumed threshold for rain production.
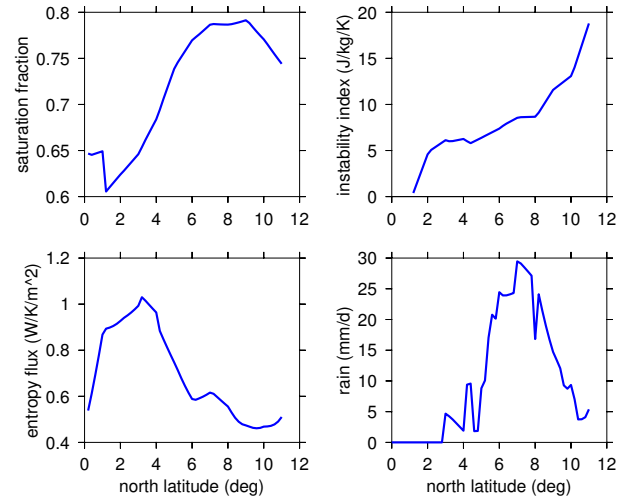
Figure 3. Time-averaged values of saturation fraction (upper left), instability index (upper right), surface moist entropy flux (lower left), and rainfall rate R_3 computed from (5).

at least qualitatively representative of the actual averaged rain.

In interpreting the rainfall plot, it is important to recall that the thresholding on rain associated with large values of DCIN and small values of instability index is applied before the time averaging. The decrease in rainfall south of 8° N is due partly to this thresholding and partly due to the decrease of saturation fraction. However, the decrease north of this point is due primarily to the steep increase in instability index there. Variations in the surface moist entropy flux contribute only weakly to this decrease. Thus, variations in the instability index, saturation fraction, and the deep convective inhibition appear to exert the primary control over convective rainfall in this region.

Raymond et al. [2015] attribute variations in instability index to the potential vorticity pattern in the atmosphere. In regions of flat SST, these variations produce a unique pattern of balanced potential temperature perturbations. Since saturated moist entropy is a function of only temperature and pressure, the instability index pattern is therefore uniquely determined by the potential vorticity, assuming that the flow is dynamically balanced and that virtual temperature effects are unimportant. However, strong SST gradients engender corresponding temperature gradients in the atmospheric boundary layer. These gradients have an important effect on the potential vorticity inversion and can therefore affect the pattern of instability index. The relative vorticity is weak in the averaged data, so the boundary layer potential temperature gradients appear to be more important in this case.

4. Conclusions

The east Pacific ITCZ is located (for most of the year) over a strong, meridional SST gradient that drives cross-equatorial southerly winds below 900 hPa. These winds terminate in a region of convergence that is thought to result from Ekman balance (sometimes extended to include downward momentum transfer from above the boundary layer) and is generally identified with the ITCZ. However, data from the EPIC2001 project demonstrate that two circulations exist in this region, with a northerly return flow located near 850 hPa associated with shallow, planetary boundary layer convection, and a deeper northerly flow in the middle to upper troposphere fed by deep convection [*Zhang et al.*, 2004]. The shallow circulation dominates in convectively suppressed situations but disappears in the presence of intense deep convection. With more moderate convection, the two can coexist [*Raymond et al.*, 2006].

On the average, boundary layer convergence is spread over a broad range of latitudes along 95° W, from 4° N to 10° N in EPIC2001 data [*Raymond et al.*, 2006]. Yet, the average satellite infrared brightness temperature exhibits a sharp negative peak near 8° N, suggesting that Ekman convergence is not the whole story in the forcing of deep convection in this region.

Further evidence comes from considering individual EPIC2001 case studies. In particular, the strongly convective case of 23 September 2001 exhibited a much deeper than normal inflow from the south as well as significant disagreement between the boundary layer convergence predicted by Ekman balance and the actual region of convergence. On the other hand, the convectively suppressed case of 2 October 2001 exhibited no deep convection at all, even though there was a robust shallow circulation that was well predicted by Ekman balance.

Recent work studying convection in tropical waves and depressions [*Raymond et al.*, 2014] as well as weak temperature gradient cloud modeling [*Raymond and Flores*, 2016] suggest that deep convective precipitation is controlled by thermodynamic factors including the surface moist entropy flux, the instability index, and the saturation fraction.

This paper shows that application of these ideas to the east Pacific ITCZ region using EPIC2001 data provides a plausible explanation for the sharp minimum in infrared brightness temperature near 8° N in this region. In particular, large values of deep convective inhibition and decreasing saturation fraction south of this latitude as well as increasing values of the instability index to the north explain the suppression of convection and precipitation away from the 7°-8° N band using the algorithm of *Raymond and Flores* [2016].

Given that the top-heaviness of convection increases with increasing instability index [*Raymond et al.*, 2014, 2015], our model predicts that convective mass flux profiles should be bottom-heavy in the heart of the ITCZ and more top-heavy to the north over warmer SSTs.

To make further progress, we need measurements of convective mass flux profiles in the various regions of the east Pacific. Existing estimates of these profiles are inconsistent and unreliable [*Back and Bretherton*, 2006, 2009b; *Handlos and Back*, 2014; *Huaman and Takahashi*, 2016]. Application to the east Pacific of observational techniques developed in recent field programs [*Raymond et al.*, 2011; *Gjorgjievska and Raymond*, 2014] would resolve these questions.

References

Back, L, E., and C. S. Bretherton, (2006), Geographic variability in the export of moist static energy and vertical motion profiles in the tropical Pacific, *Geophys. Res. Letters*, *33*, L17810, doi:10.1029/2006GL026672.

Back, L. E., and C. S. Bretherton, (2009a), On the relationship between SST gradients, boundary layer winds, and convergence over the tropical oceans, *J. Climate*, *33*, 4182-4196.

Back, L. E., and C. S. Bretherton, (2009b), A simple model of climatological rainfall and vertical motion patterns over the tropical oceans, *J. Climate*, *22*, 6477-6497.

Battisti, D. S., E. S. Sarachik, and A. C. Hirst, (1999), A consistent model for the large-scale steady surface atmospheric circulation in the tropics, *J. Climate*, *12*, 2956-2964.

Bretherton, C. S., M. E. Peters, and L. E. Back, (2004), Relationships between water vapor path and precipitation over the tropical oceans, *J. Climate*, *17*, 1517-1528.

Daleu, C. L., R. S. Plant, S. J. Woolnough, S. Sessions, M. J. Herman, A. Sobel, S. Wang, D. Kim, A. Cheng, G. Bellon, P. Peyrille, F. Ferry, P. Siebesma, and L. Van Ulft, (2015), Intercomparison of methods of coupling between convection and large-scale circulation: 1. Comparison over uniform surface conditions, *J. Adv. Model. Earth Syst.*, *7*, doi:10.1002/2015MS000468.

Emanuel, K. A., (1986), An air-sea interaction theory for tropical cyclones: Part I: Steady state maintenance, *J. Atmos. Sci.*, *43*, 585-604.

Emanuel, K. A., (1987), An air-sea interaction model of intraseasonal oscillations in the tropics, *J. Atmos. Sci.*, *44*, 2324-2340.

Emanuel, K. A., (1995), The behavior of a simple hurricane model using a convective scheme based on subcloud-layer entropy equilibrium, *J. Atmos. Sci.*, *52*, 3960-3968.

Gjorgjievska, S., and D. J. Raymond, (2014), Interaction between dynamics and thermodynamics during tropical cyclogenesis, *Atmos. Chem. Phys.*, *14*, 3065-3082.

Handlos, Z. J., and L. E. Back, (2014), Estimating vertical motion profile shape within tropical weather states over the oceans, *J. Climate*, *27*, 7667-7686.

Herman, M. J., and D. J. Raymond, (2014), WTG Cloud modeling with spectral decomposition of heating. *J. Adv. Model. Earth Syst.*, *6*, 1121-1140, doi:10.1002/2014MS000359.

Huaman, L., and K. Takahashi, (2016), The vertical structure of the eastern Pacific ITCZs and associated circulation using the TRMM precipitation radar and *in situ* data, *Geophys. Res. Letters*, *43*, 8230-8239, doi:10.1002/2016GL068835.

Lindzen, R. S., and S. Nigam, (1987), On the role of sea surface temperature gradients in forcing low-level winds and convergence in the tropics, *J. Atmos. Sci.*, *44*, 2418-2436.

Miller, M. J., A. C. M. Beljaars, and T. N. Palmer, (1992), The sensitivity of the ECMWF model to the parameterization of evaporation from the tropical oceans, *J. Climate*, *5*, 418-434.

Neelin, J. D., I. M. Held, and K. H. Cook, (1987), Evaporation-wind feedback and low-frequency variability in the tropical atmosphere, *J. Atmos. Sci.*, *44*, 2341-2348.

Peters, O., and J. D. Neelin, (2006), Critical phenomena in atmospheric precipitation. *Nature Physics*, *2*, 393-396, doi:10.1038/nphys314.

Petersen, W. A., R. Cifelli, D. J. Boccippio, S. A. Rutledge, and C. Fairall, (2003), Convection and easterly wave structures observed in the eastern Pacific warm pool during EPIC-2001, *J. Atmos. Sci.*, *60*, 1754-1773.

Raymond, D. J., (1995), Regulation of moist convection over the west Pacific warm pool, *J. Atmos. Sci.*, *52*, 3945-3959.

Raymond, D. J., (2000), Thermodynamic control of tropical rainfall, *Quart. J. Roy. Meteor. Soc.*, *126*, 889-898.

Raymond, D. J., S. K. Esbensen, C. Paulson, M. Gregg, C. S. Bretherton, W. A. Petersen, R. Cifelli, L. K. Shay, C. Ohlmann, and P. Zuidema, (2004), EPIC2001 and the coupled ocean-atmosphere system of the tropical east Pacific, *Bull. Am. Meteor. Soc.*, *85*, 1341-1354.

Raymond, D. J., C. S. Bretherton, and J. Molinari, (2006), Dynamics of the intertropical convergence zone of the east Pacific, *J. Atmos. Sci.*, *63*, 582-597.

Raymond, D. J., and M. M. Flores, (2016), Predicting convective rainfall over tropical oceans from environmental conditions. *J. Adv. Model. Earth Syst.*, *8*, doi:10.1002/2015MS000595.

Raymond, D. J., Ž. Fuchs, S. Gjorgjievska, and S. L. Sessions, (2015), Balanced dynamics and convection in the tropical troposphere, *J. Adv. Model. Earth Syst.*, *7*, doi:10.1002/2015MS000467.

Raymond, D. J., S. Gjorgjievska, S. Sessions, and Ž. Fuchs, (2014), Tropical cyclogenesis and mid-level vorticity, *Australian Meteorological and Oceanographic Journal*, *64*, 11-25.

Raymond, D. J., G. B. Raga, C. S. Bretherton, J. Molinari, C. López-Carrillo, and Ž. Fuchs, (2003), Convective forcing in the intertropical convergence zone of the eastern Pacific, *J. Atmos. Sci.*, *60*, 2064-2082.

Raymond, D. J. and S. L. Sessions, (2007), Evolution of convection during tropical cyclogenesis, *Geophys. Res. Letters*, *34*, L06811, doi:10.1029/2006GL028607.

Raymond, D. J., S. L. Sessions, and C. López Carrillo, (2011), Thermodynamics of tropical cyclogenesis in the northwest Pacific, *J. Geophys. Res.*, *116*, D18101, doi:10.1029/2011JD015624.

Raymond, D. J., and X. Zeng, (2005), Modelling tropical atmospheric convection in the context of the weak temperature gradient approximation, *Quart. J. Roy. Meteor. Soc.*, *131*, 1301-1320.

Riehl, H., T. C. Yeh, J. S. Malkus and N. E, La Seur, (1951), The north-east trade of the Pacific ocean, *Quart. J. Roy. Meteor. Soc.*, *77*, 598-626.

Singh, M. S., and P. A. O'Gorman, (2013), Influence of entrainment on the thermal stratification in simulations of radiative-convective equilibrium, *Geophys. Res. Letters*, *40*, 4398-4403.

Stevens, B., J. Duan, J. C. McWilliams, M. Munnich, and J. D. Neelin, (2002), Entrainment, Rayleigh friction, and boundary layer winds over the tropical Pacific, *J. Climate*, *15*, 30-44.

Tomas, R. A., J. R. Holton, and P. J. Webster, (1999), The influence of cross-equatorial pressure gradients on the location of near-equatorial convection, *Quart. J. Roy. Meteor. Soc.*, *125*, 1107-1127.

Yano, J.-I., and K. Emanuel, (1991), An improved model of the equatorial troposphere and its coupling with the stratosphere, *J. Atmos. Sci.*, *48*, 377-389.

Zhang, C., M. McGauley, and N. A. Bond, (2004), Shallow meridional circulation in the tropical eastern Pacific, *J. Climate*, *17*, 133-139.

―――――――
Corresponding author: D. J. Raymond, Physics Department and Geophysical Research Center, New Mexico Tech, Socorro, NM 87801, USA. (david.raymond@nmt.edu)